Heteronuclear NMR Studies of the Combined Src Homology Domains 2 and 3 of pp60 c-Src: Effects of Phosphopeptide Binding†

Marco Tessari,‡ Lisa N. Gentile,§,|| Stephen J. Taylor,§ David I. Shalloway,§ Linda K. Nicholson,*,§ and Geerten W. Vuister*,‡,⊥

Department of NMR Spectroscopy, Bijvoet Center for Biomolecular Research, Utrecht University, Padualaan 8, 3584 CH Utrecht, The Netherlands, and Section of Biochemistry, Molecular and Cell Biology, Cornell University, 239 Biotechnology Building, Ithaca, New York 14853

Received May 22, 1997; Revised Manuscript Received September 15, 1997⊗

ABSTRACT: The results of heteronuclear NMR studies on the combined Src homology domains 2 and 3 (SH3-SH2) of pp60 c-Src are presented. Resonance assignments were obtained using heteronuclear triple-resonance experiments in conjunction with ^{15}N-separated nuclear Overhauser effect spectroscopy (NOESY) data. A modified three-dimensional ^{13}CO−^{15}N−^{1}H spectral correlation experiment [(HACA)CO(CA)-NH] with improved sensitivity is presented that provided additional sequential information and resolved several ambiguities. Chemical shifts and sequential- and medium-range NOE cross peaks indicate that the structures of both the SH3 and SH2 portions of the polypeptide are very similar to those of the isolated SH3 and SH2 domains. Binding of a high-affinity phosphopeptide, EPQpYEEIPIYL, induces large chemical shift changes at several locations in the SH2 domain. Comparison with known results for peptide binding to SH2 domains shows that the residues displaying the largest effects are all involved in peptide binding or undergo significant conformational changes upon binding. However, subtle changes of both ^{1}H and ^{15}N chemical shifts are observed for residues within the SH3 domain and the connecting linker region, indicating possible cross-domain communication.

A series of exciting discoveries during the past few years has shown that protein tyrosine phosphorylation plays an essential role in linking extracellular signaling events to intracellular signal transduction cascades (Hunter, 1995). Tyrosine kinases that pass the signal from the inner surface of the plasma membrane to downstream effectors within the cell fall into two general categories: membrane-bound receptors that possess intrinsic tyrosine kinase activity and nonreceptor tyrosine kinases that transiently couple via modular binding domains to receptors that lack their own tyrosine kinase activity. One such membrane-associated nonreceptor protein tyrosine kinase (PTK)[1] is c-Src, a protooncoprotein that is the prototype for the nine proteins of the Src family of PTKs [for a review see Superti-Furga and Courtneidge (1995)], which are involved in a diverse array of signaling pathways.

All nine PTKs of the Src family have similar sequences that can be divided into six regions: a myristylation site near the amino terminus, a variable region unique to each family member, a Src homology 3 (SH3) domain, a Src homology 2 (SH2) domain, a tyrosine kinase domain, and a short carboxyl-terminal tail containing a key regulatory tyrosine residue (Pawson, 1992). The SH2 and SH3 domains are small globular domains that are found in a wide range of functionally diverse proteins. They serve important roles in signal transduction by mediating specific inter- and intramolecular protein−protein interactions [for reviews see Pawson (1992), Kuriyan and Cowburn (1993), and Schaffhausen et al. (1995)]. The tertiary structures of isolated SH3 and SH2 domains have been well studied by both X-ray crystallography (Waksman et al., 1992, 1993; Musacchio et al., 1992, 1994; Eck et al., 1993; Lee et al., 1994; Noble et al., 1993) and NMR spectroscopy (Yu et al., 1992, 1993; Booker et al., 1992, 1993; Overduin et al., 1992; Kohda et al., 1993; Koyama et al., 1993; Pascal et al., 1994; Xu et

† G.W.V. has been financially supported by the Royal Netherlands Academy of Arts and Sciences (KNAW). L.K.N. and this work have been largely supported by The National Science Foundation, Grants MCB-9507144 and BIR-9512501.

* To whom correspondence should be addressed.

‡ Utrecht University.

§ Cornell University.

|| Present address: 2146 Health Sciences Mall, Department of Biochemistry, University of British Columbia, Vancouver, BC V6T1Z3, Canada.

⊥ Present address: Nijmegen SON Research Center, Laboratory of Biophysical Chemistry, University of Nijmegen, Toernooiveld, 6525 ED Nijmegen, The Netherlands.

⊗ Abstract published in *Advance ACS Abstracts,* November 1, 1997.

[1] Abbreviations: CBCA(CO)NH, three-dimensional (^{13}C$^{\alpha}$,^{13}C$^{\beta}$)−^{15}N−^{1}H spectrum correlating amide ^{1}H and ^{15}N with C$^{\alpha}$ and C$^{\beta}$ shifts of the preceding residue; CBCANH, three-dimensional (^{13}C$^{\alpha}$,^{13}C$^{\beta}$)−^{15}N−^{1}H spectrum correlating amide ^{1}H and ^{15}N with sequential and intraresidue C$^{\alpha}$ and C$^{\beta}$ shifts; CT, constant time; HA(CACO)NH, three-dimensional ^{1}H$^{\alpha}$−^{15}N−^{1}H spectrum correlating amide ^{1}H and ^{15}N with sequential H$^{\alpha}$ shift; (HACA)CO(CA)NH, three-dimensional ^{13}CO−^{15}N−^{1}H spectrum correlating amide ^{1}H and ^{15}N with sequential and intraresidue CO shifts; HNCA, three-dimensional ^{13}C$^{\alpha}$−^{15}N−^{1}H spectrum correlating amide ^{1}H and ^{15}N with sequential and intraresidue C$^{\alpha}$ shifts; HNCACB, three-dimensional (^{13}C$^{\alpha}$,^{13}C$^{\beta}$)−^{15}N−^{1}H spectrum correlating amide ^{1}H and ^{15}N with sequential and intraresidue C$^{\alpha}$ and C$^{\beta}$ shifts; HN(CA)HA, three-dimensional ^{1}H$^{\alpha}$−^{15}N−^{1}H spectrum correlating amide ^{1}H and ^{15}N with sequential and intraresidue H$^{\alpha}$ shifts; HNCO, three-dimensional ^{13}CO−^{15}N−^{1}H spectrum correlating amide ^{1}H and ^{15}N with the CO shift of the preceding residue; HN(CO)CA, three-dimensional ^{13}C$^{\alpha}$−^{15}N−^{1}H spectrum correlating amide ^{1}H and ^{15}N with sequential C$^{\alpha}$ shift; HSQC, heteronuclear single quantum correlation; MQ, multiple-quantum; MQ-SE, spin-locked multiple-quantum sensitivity-enhanced experiment; NMR, nuclear magnetic resonance; NOE, nuclear Overhauser effect; NOESY, two-dimensional nuclear Overhauser effect spectroscopy; PFG, pulsed field gradient; PTK, protein tyrosine kinase; pY, phosphorylated tyrosine; SH2, Src homology domain 2; SH3, Src homology domain 3; SH(32), combined SH3-SH2 domains.

S0006-2960(97)01204-X CCC: $14.00

al., 1995, Gosser et al., 1995; Hiroaki et al., 1996). SH3 domains form a compact β-barrel structure composed of two short, approximately perpendicular, three-stranded antiparallel β-sheets.[2] SH3 domains bind peptides containing the Pro-X-X-Pro motif (X is any residue). The ligand forms a left-handed polyproline-II helix and binds across one side of the SH3 β-barrel along a shallow hydrophobic groove (Kuriyan & Cowburn, 1993). Two classes of ligands have emerged from combinatorial peptide library screening (Feng et al., 1994) that differ in the position of a key Arg residue relative to the Pro-X-X-Pro motif. This distinction determines the orientation of ligand binding through a salt bridge with a conserved Asp residue within the SH3 domain.

The SH2 structural motif consists of a large central β-sheet flanked by two α-helices, and a second smaller β-sheet.[2] SH2 domains bind to phosphotyrosine-containing sequences through two binding pockets on the SH2 surface, one that has high affinity for phosphotyrosine and a second that imparts sequence specificity and distinguishes SH2 domains into two classes. Members of the first class, which includes the SH2 domain of Src, bind to peptides containing the pTyr-hydrophilic-hydrophilic-Ile/Pro motif, whereas members of the second class bind to peptides containing the pTyr-hydrophobic-X-hydrophobic motif (Songyang et al., 1994). The sequence specificity of the individual SH2 domains has been shown to depend on the three residues C-terminal to the pTyr (Songyang et al., 1993, 1994) and can be modified by substitution of a single residue in the second binding pocket (Marengere et al., 1994). Structural studies of SH2/ligand complexes (Pascal et al., 1994; Waksman et al., 1992, 1993; Eck et al., 1993, 1994) and mutagenesis studies (Yoakim et al., 1994) have further revealed the importance of specific interactions between the SH2 and high-affinity phosphopeptides in determining sequence specificity.

The functional importance of the Src SH3 and SH2 domains in regulating c-Src activity has been addressed by numerous biochemical and genetics studies. A direct role of SH2 in maintaining the repressed state of the kinase via intramolecular association with the phosphorylated C-terminal regulatory tyrosine is now well established (Stover et al., 1994). However, the mechanism of SH3 regulation of Src kinase activity, implicated in numerous mutational studies (Hirai & Varmus, 1990; Okada et al., 1993; Kato et al., 1986; Seidel-Dugan et al., 1992; Murphy et al., 1993; Superti-Furga et al., 1993), was not well understood. The recent X-ray crystal structures of the repressed state of nearly intact human c-Src and Src family member Hck have confirmed the expected intramolecular interaction between the SH2 and the phosphorylated tail but have also revealed a surprising intramolecular interaction between the SH3 domain and a polyproline-II helix formed by residues linking the SH2 and kinase domains (Xu et al., 1997; Sicheri et al., 1997). This unexpected interaction alters the orientation of helix c in the kinase domain, which removes a key residue from the active site. Hence, intramolecular interactions involving the SH2 and SH3 domains and sequences flanking the kinase domain are responsible for maintaining the repressed state. Competition for either of these interactions has been shown to result in activation of kinase activity (Stover et al., 1994; Moarefi et al., 1997). Hence, in the context of the repressed state, SH3 and SH2 ligand binding affinity and specificity are of great importance in regulation of kinase activity.

Recent biochemical studies have also demonstrated physical and functional interactions between contiguous SH3 and SH2 domains that mediate their respective binding affinities. For the combined SH3-SH2 (SH(32)) domains of Fyn it was found that binding of phosphotyrosine-containing sequences by the SH2 domain was enhanced by the presence of the attached SH3 domain and that the ligand binding characteristics of each domain were sensitive to the occupancy state of the other linked domain (Panchamoorthy et al., 1994). Furthermore, direct *in vitro* association of SH3 and SH2 domains was shown between SH2 and SH3 domains of the members of the c-Src family of PTKs but not between c-Src-like SH2 domains and non-c-Src-like SH3 domains or *vice versa*. This interaction was disrupted by occupancy of the SH2 domain with a phosphopeptide ligand but not by occupancy of the SH3 domain by a Pro-rich ligand (Panchamoorthy et al., 1994). Interestingly, association between Src and its recently identified mitotic target, Sam68, also involves both the SH3 and SH2 domains (Taylor & Shalloway, 1994; Fumagalli et al., 1994; Taylor et al., 1995). Hence, allosteric interactions between contiguous SH3-SH2 domains in Src family members have been demonstrated *in vitro* and have potential functional importance in modulating interactions with upstream and/or downstream signaling molecules.

A detailed mechanism of intramolecular allosteric interactions between SH3 and SH2 domains has not yet been established. High-resolution structures of combined SH(32) domains from Abl, Grb2, and Src family member Lck have been determined by X-ray crystallography (Nam et al., 1996; Maignan et al., 1995; Eck et al., 1994). In all three cases, the global fold of each domain is essentially the same that of as the corresponding isolated domain. The Lck crystal structures of both the unliganded and phosphopeptide-bound proteins formed a head-to-tail dimer with substantial intermolecular SH3/SH2 contacts across the dimer interface with minimal intramolecular interdomain interactions; the intermolecular contact surface was not significantly perturbed by phosphopeptide binding (Eck et al., 1994). The crystal structure of unliganded Abl SH(32) is monomeric, with intramolecular van der Waals contacts between the bc and BC loops (Nam et al., 1996). These interdomain interactions were interpreted as a possible mechanism for intramolecular regulation of ligand binding. However, an NMR-derived model for the SH(32) solution structure of Abl suggests a flexible, unstructured linker region and showed no evidence for significant intramolecular SH3/SH2 interactions (Gosser et al., 1995). The crystal structure of Grb2, which consists of two SH3 and one SH2 domains, also shows no significant intramolecular SH3/SH2 interactions and suggests the possibility that Grb2 is a flexible adapter in which its binding domains could adopt different relative orientations as needed (Maignan et al., 1995).

Here, we present the results of heteronuclear multidimensional NMR studies on the combined SH(32) domains derived from chicken c-Src, for both the unliganded protein and the complex with a high-affinity phosphopeptide. The secondary structural elements for the unliganded protein

[2] Using standard nomenclature (Cohen et al., 1995), the six strands of β-sheet of SH3 are denoted by βa, βb$_1$, βb$_2$, and βc−βe, the β-strands of SH2 are denoted by βA−βG, the helices of SH2 are denoted by αA and αB, and loops are denoted by the secondary structural elements they connect.

show only minor differences with respect to the solution structures of the isolated SH3 and SH2 domains. Upon phosphopeptide binding, chemical shift and hydrogen-exchange data show that, while the largest changes in chemical environment and solvent accessibility occur in expected regions of the SH2 domain, subtle but significant changes are observed at sites within the SH3 domain and the connecting linker. These results suggest a direct mechanism for interdomain communication that might facilitate allosteric regulation of the Src regulatory apparatus.

EXPERIMENTAL PROCEDURES

The pGEX-5H expression vector encodes a fusion protein composed of glutathione S-transferase (GST), a thrombin cut site, and the combined c-Src SH3 and SH2 domains. This vector was constructed by *Bsa*HI and *Mlu*I restriction digests of a c-Src-encoding plasmid, pM5H (Lin et al., 1995), and subsequent ligation of the appropriate fragment into the *Sma*I site of pGEX-2T (Pharmacia). The pGEX-5H vector yields a protein product which, after cleavage with thrombin, contains c-Src residues 83−259 and non-c-Src residues Gly-Ser-Pro and Asn-Ser-Ser at the N- and C-termini, respectively. The last eight residues on the C-terminus proved to be labile and were lost from the protein as a function of sample lifetime (complete after approximately 8 days). The shortened polypeptide, hereafter referred to as SH(32), has a total of 175 amino acids (containing c-Src residues 83−254) with a theoretical mass of 19.8 kDa.

The pGEX-5H vector was transformed into *E. coli* BL21(DE3) cells. Uniformly labeled ^{15}N and $^{15}N/^{13}C$ samples were prepared by growing transformed *E. coli* on M9 minimal medium containing [$^{13}C_6$]glucose (Cambridge Isotope Labs) and/or $^{15}NH_4Cl$ (Isotec) as the sole carbon and nitrogen sources, respectively. One liter of cell culture in a 3 L Fernbach flask was vigorously agitated at 37 °C, protein expression was induced with IPTG at $OD_{600} = 0.35$, and after 4 h the cells were pelleted and washed in PBS (140 mM NaCl, 2.7 mM KCl, 10 mM Na_2HPO_4, and 1.8 mM KH_2PO_4). The pellet was resuspended in 10 mL of lysis buffer (25 mM HEPES, pH = 7.5, 150 mM NaCl, 1 mM EDTA, 0.2 mM DTT, 1 μg/mL aprotinin, 0.5 μM leupeptin, and 1 μM pepstatin A), and the cells were ruptured by two passes through a French pressure cell. The crude cell lysate was centrifuged (1 h at 35*g*), and the supernatant was further clarified by passage through a 0.8 μm filter and was then applied to a glutathione (GSH) agarose affinity column (Pharmacia) equilibrated in lysis buffer at 4 °C. All subsequent purification steps were carried out at 4 °C unless otherwise noted. The GSH column was washed with 10 bed volumes of PBS, and the GST−SH(32) fusion protein was eluted with 5 bed volumes of elution buffer (10 mM reduced glutathione in 50 mM Tris-HCl, pH = 8.0). An additional 2.5 bed volumes of elution buffer were added to the column, and the column was capped, turned end-over-end for 12 h, and then rinsed with 1.5 bed volumes of elution buffer and 1.5 bed volumes of PBS. The initial and overnight elution volumes were pooled, and the pure fusion protein was concentrated to 1 mg/mL and exchanged into thrombin cut buffer (20 mM Tris-HCl, 100 mM NaCl, and 2 mM $CaCl_2$, pH = 8.5) using Centriprep 10 concentrators (Amicon, Inc.). Incubation with 0.25 unit of thrombin (Boehringer Mannheim) for 12 h at 4 °C resulted in complete cleavage of the fusion protein. The cut reaction was subsequently passed through a *p*-aminobenzamidine−Sepharose column (Sigma) equilibrated in thrombin cut buffer to extract the thrombin. The solution was then reapplied to the glutathione affinity column to remove the detached GST, and the flowthrough containing pure SH(32) was exchanged into NMR buffer (50 mM Na_2HPO_4, 200 mM Na_2SO_4, and 10 mM DTT, pH 6.4) and concentrated. This procedure yielded on average approximately 10 mg of pure protein from 1 L of bacterial culture. The purified protein was characterized by mass spectrometry and N-terminal sequencing (which verified the first seven residues), and purity was determined by analytical HPLC to be approximately 98%.

NMR. All NMR experiments were recorded on 0.8 or 1.0 mM protein solutions in 90%/10% (v/v) H_2O/D_2O, 50 mM Na_2HPO_4, 200 mM Na_2SO_4, and 10 mM DTT, pH 6.4, using a microcell NMR tube (Shigemi Inc., Allison Park, PA). The spectra were acquired at 25 or 30 °C using Bruker AMX2 600, Varian UnityPlus 500 and 750, and Unity INOVA 600 spectrometers, all equipped with triple-resonance probe heads and self-shielded *z*-gradients. The NMR experiments used for the assignments are listed in Table 2 of the supporting information. All original versions of the experiments were modified to include water flip-back pulses (Grzesiek & Bax, 1993; Stonehouse et al., 1994; Kay et al., 1994) to avoid saturation transfer between H_2O protons and the amide protons, as well as sensitivity enhancement in conjunction with gradient coherence selection (Kay et al., 1992a; Muhandiram & Kay, 1994). The (HACA)CO(CA)NH experiment originally proposed by Löhr and Rüterjans (1995) was modified as described below.

NMR spectra were processed using the NMRPipe software package (Delaglio et al., 1995). Typically, in the acquisition dimension the small residual H_2O resonance was removed by a solvent-suppression time domain filter (Marion et al., 1989), apodized by a 72° shifted squared sine-bell window, zero-filled once, and Fourier-transformed. In the indirectly detected dimensions the data were apodized by a 72° shifted squared sine-bell window function, zero-filled twice, and Fourier transformed. For the constant-time triple-resonance experiments the length of the nondecaying ^{15}N time-domain data was doubled by mirror-image linear prediction (Zhu & Bax, 1990), apodized, zero-filled once, and Fourier-transformed. Data analysis was performed using the program PIPP (Garret et al., 1991) or REGINE (Kleywegt et al., 1993). Both programs use parabolic interpolation in all dimensions for determining the peak positions.

RESULTS AND DISCUSSION

Assignment. Assignment of the backbone resonances of SH(32) were obtained from the analysis of three-dimensional triple-resonance spectra in conjunction with ^{15}N- and ^{13}C-separated NOE spectra (cf. Table 2 in the supporting information). This procedure relies primarily upon experiments that detect the amide proton. The $^{15}N-^{1}H$ HSQC spectrum, recorded with a large $t_{1,max}$ of 112 ms, is shown in Figure 1. As can be expected for a protein with 175 residues, there is significant overlap in $^{15}N-^{1}H$ frequency space, complicating the assignment procedure. In several instances resonances overlap within their line widths, e.g., Tyr^{13} and Ala^{59} or Tyr^{57}, Asn^{88}, Gln^{146}, and Val^{148}. In addition, the intensities of the resonances of the structured portion of the protein span over 1 order of magnitude,

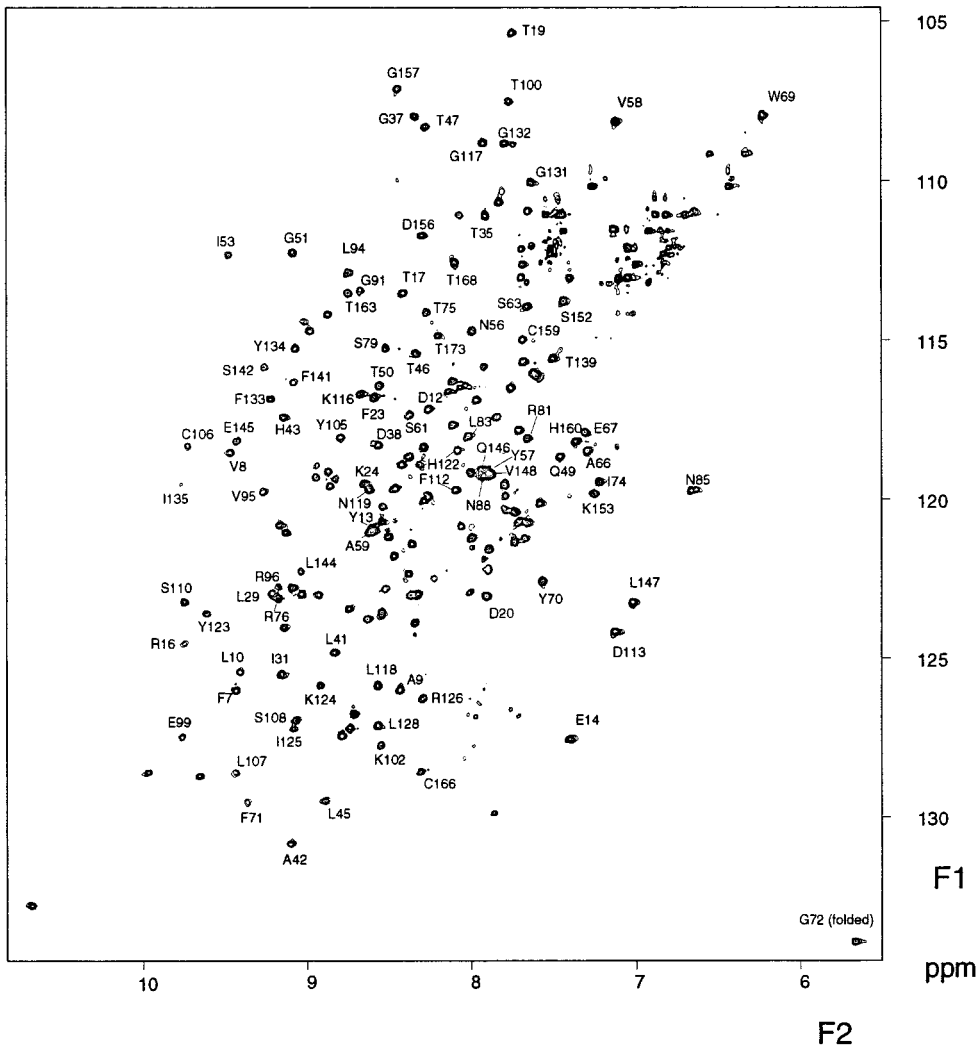

FIGURE 1: ^{15}N HSQC spectrum ($F1 = {}^{15}N$, $F2 = {}^{1}H$) of a 0.8 mM solution in H_2O of uniformly ^{15}N-labeled SH(32) of pp60 c-Src recorded at 750 MHz ^{1}H resonance frequency. Selected residues of SH(32) are indicated.

indicating a wide variation in dynamics across the backbone. Moreover, for several residues in loop regions no correlations could be identified and hence Asn[114], Asp[129], Ser[130], Arg[161], and Leu[162] remain unassigned. Since the H_2O magnetization is kept close to its thermal equilibrium value during the $^{15}N-{}^{1}H$ HSQC experiment, rapid exchange with the H_2O cannot account for the absence or decrease of signal intensities as observed for several amides. Rather, these residues could be subject to conformational exchange that is intermediate on the NMR time scale.

The combined use of the HNCA/HN(CO)CA (Ikura et al., 1990; Bax & Ikura, 1991; Grzesiek & Bax, 1992a) and HN(CA)HA/HN(COCA)HA triple-resonance spectra (Clubb et al., 1992a; Clubb & Wagner, 1992; Kay et al., 1992b) allows the identification of sequential links through the C^{α} and H^{α} resonances, respectively. However, the spectral dispersion of the $^{13}C^{\alpha}-{}^{1}H^{\alpha}$ correlation map is in general insufficient to unambiguously establish full sequential connectivities. Relay to the C^{β} nucleus by means of the CBCA(CO)NH/CBCANH or HN(CA)CB experiments (Grzesiek & Bax, 1992b,c; Wittekind & Mueller, 1993) provides an independent spin that can be used for establishing the sequential connectivities.

An alternative approach uses the CO nucleus through the HNCO/HN(CA)CO experiments. The HNCO experiment, which correlates C'_{i-1} with $^{1}H_i$ and $^{15}N_i$, is the most sensitive triple-resonance experiment. Unfortunately, the HN(CA)-CO experiment (Clubb et al., 1992b), which provides the sequential link correlating both C'_{i-1} and C'_i to $^{1}H_i$ and $^{15}N_i$, has an inherently low sensitivity. The (HACA)CO(CA)NH experiment (Löhr & Rüterjans, 1995) was proposed as an improvement of the HN(CA)CO experiment for medium-sized proteins. Here, we present a modification of this latter experiment, which yields spectra with improved sensitivity and spectral quality.

The pulse sequence for the spin-locked MQ sensitivity-enhanced (HACA)CO(CA)NH experiment [MQ-SE-(HACA)-CO(CA)NH] is shown in Figure 2. The general course of the magnetization transfer is as described by Löhr and Rüterjans (1995) and will not be reiterated in detail. Very briefly, H^{α} magnetization is transferred to its directly attached C^{α} nucleus. During a constant-time period of $2T$, the C^{α} magnetization dephases with respect to the CO nucleus, is frequency-labeled with the CO chemical shift in a semi-constant time HMQC fashion, and rephased. The 2T period is chosen to allow for a complete refocusing of the $^{1}J(CC)$ couplings. Simultaneously, during the $2T$ period the C^{α} magnetization dephases with respect to the intraresidual and sequential nitrogen nuclei as a result of $^{1}J(C^{\alpha}N)$ and $^{2}J(C^{\alpha}N)$ couplings, respectively. Subsequently, INEPT-type transfer to the nitrogen is followed by reverse-INEPT transfer to the amide protons, which are detected during acquisition in t_3.

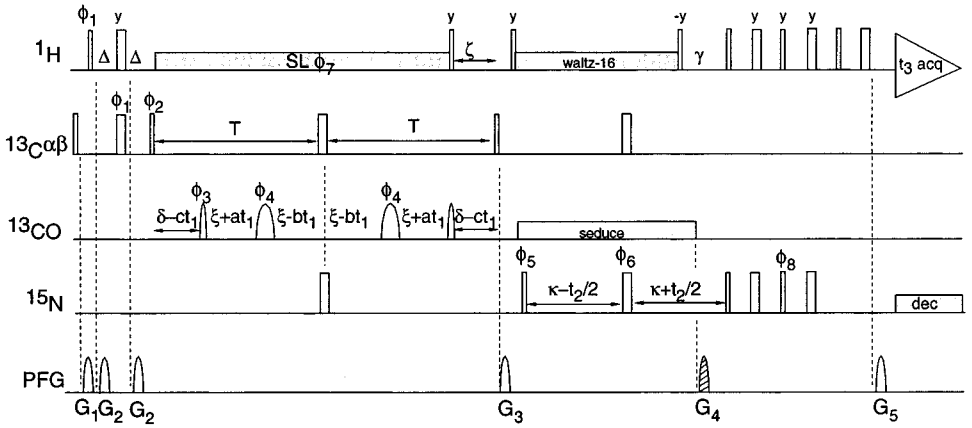

FIGURE 2: Pulse sequence of the spin-locked MQ sensitivity-enhanced (HACA)CO(CA)NH experiment. Narrow and wide bars denote pulses with a 90° and 180° flip angle, respectively. ^{1}H 90° and 180° pulses on the ^{13}C channel during 2T have a zero-excitation profile at the center of the carbonyl frequency. CO pulses are implemented as off-resonance Gaussian pulses with a duration of 153.6 μs for a 90° pulse. The ^{13}C carrier is placed in the center of the aliphatic region (43 ppm) during the 2T period and shifted to the C$^\alpha$ region during the 2κ period. All pulses are applied along the x-axis unless indicated otherwise. The phases are as follows: $\phi_1 = x, -x$; $\phi_2 = 2x, 2(-x)$; $\phi_3 = 4x, 4(-x)$; $\phi_4 = 8x, 8(-x)$; $\phi_5 = 8x, 8(-x)$; $\phi_6 = 2x, 2(-x)$; $\phi_7 = 2x, 2(-x)$; $\phi_8 = -y$; receiver = $P, -P, -P, P$ with $P = x, 2(-x), x$. Pulsed field gradients (PFG) had a sine-bell shape and were applied along the z-axis. Duration and strength of the gradients were as follows: $G_1 = 1$ ms, −15 G/cm; $G_2 = 1$ ms, 7 G/cm, $G_3 = 1$ ms, 20 G/cm; $G_4 = 2.0$ ms, 30 G/cm; and $G_5 = 1$ ms, 6.08 G/cm. PFGs G_2 are used to remove imperfections resulting from the 180° pulses. PFG G_3 is used for purging transversal magnetization terms and selecting for $C^\alpha_z N_z$ spin-order, whereas gradients G_4 and G_5 are used for sensitivity-enhanced gradient-coherence selection in the manner described by Kay et al. (1992). Gradient G_4 was alternated in sign and phase ϕ_8 incremented by 180° on successive FIDs in order to record P- and N-type spectra. Postacquisition data processing yields cosine and sine-modulated data in t_2. Quadrature detection in t_1 was obtained using the States-TPPI method incrementing phase ϕ_3. Semiconstant time in t_1 was employed setting a, b, and c to 0.335, 0.165, and 0.17, respectively. The delays were as follows: $\Delta = 1.75$ ms, $T = 14.3$ ms, $\delta = 9.09$ ms, $\xi = 2.605$ ms, $\zeta = 2.4$ ms, $\kappa = 12.4$ ms, and $\gamma = 5.4$ ms. ^{1}H spin-lock (SL) and WALTZ-16 decoupling were achieved using RF field strengths of 3.5 and 7.6 kHz, respectively. ^{13}C decoupling during t_2 was accomplished using a SEDUCE decoupling scheme (McCoy & Mueller, 1992) with a 2.9 kHz RF field strength. ^{15}N decoupling during acquisition was accomplished using the WALTZ-16 decoupling scheme (Shaka et al., 1983) with an RF field strength of 1.25 kHz.

Modifications of the original scheme include the now-standard application of pulsed-field gradients (PFG) for suppression of artifacts resulting from unwanted coherence-transfer pathways and for sensitivity enhancement (Vuister et al., 1991; Boyd et al., 1992; Davis et al., 1992; Kay et al., 1992a). The unique modification is the introduction of a spin-lock multiple-quantum (MQ) scheme (Grzesiek & Bax, 1995) during the 2T constant-time period. In the original scheme the magnetization resided on the C$^\alpha$ nucleus, which has a notoriously short transverse relaxation time resulting predominantly from the strong ^{13}C$^\alpha$−^{1}H$^\alpha$ dipolar interaction. Considerable improvement in sensitivity is obtained by maintaining the magnetization as ^{13}C$^\alpha$−^{1}H$^\alpha$ heteronuclear MQ since, in the slow tumbling limit, relaxation of these terms is not affected by the dipolar interaction (Griffey & Redfield, 1987). Application of a proton spin-lock field, during the $2T - \zeta$ period, suppresses the evolution of proton−proton J-coupling terms. The subsequent $90°_y$ pulse generates C$^\alpha$ magnetization antiphase with respect to its directly attached H$^\alpha$, which refocuses to in-phase C$^\alpha$ magnetization during the delay ζ. As in the original scheme, the transverse C$^\alpha$ component simultaneously dephases with respect to the intraresidue and sequential ^{15}N spins as a result of ^1J(C$^\alpha$N) and ^2J(C$^\alpha$N) couplings, respectively.

Strips along the ^{13}CO axis taken at the ^{15}N−^{1}H resonance frequencies of Asn^{119} through Lys^{124} of the CT-HNCO and MQ-SE-(HACA)CO(CA)NH spectra of uniformly ^{13}C/^{15}N-labeled SH(32) of pp60 c-Src in H_2O solution are shown in Figure 3. The PFG-SE scheme yields ca. 20−40% increase in sensitivity as compared to the original (HACA)CO(CA)-NH experiment, in accordance with the gain of 1.2−1.4 in sensitivity typically observed for proteins of this size (Muhandiram & Kay, 1994; Kay et al., 1994). The sensitivity improvement resulting from spin-locking the MQ coherence was checked by comparing $F_2 - F_3$ ^{15}N−^{1}H spectra of the non-spin-locked version (PFG-SE included) with the spin-locked version of the experiment (Figure 2). Comparison of ca. 15 randomly chosen cross peaks indicated a sensitivity gain of 30−40% (data not shown). Overall, the sensitivity has increased 60−100% in our modified scheme with respect to the original experiment of Löhr and Rütherjans (1995).

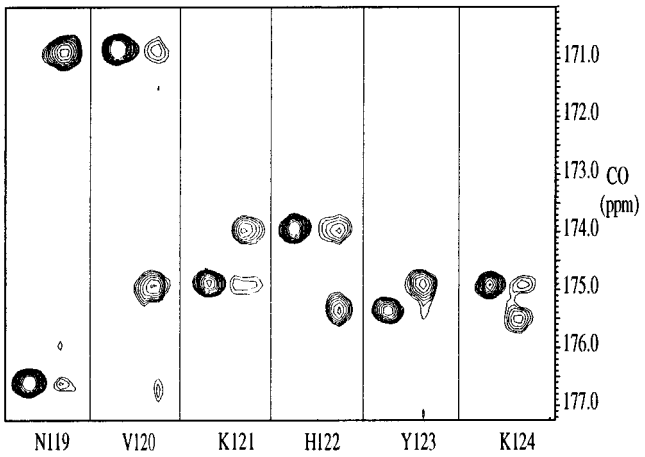

FIGURE 3: Strip plots from the three-dimensional HNCO and three-dimensional MQ-SE-(HACA)CO(CA)NH spectra (left and right part of each panel, respectively) of a 1.0 mM solution in H_2O of uniformly ^{13}C/^{15}N-labeled SH(32), taken at the ^{15}N/^{1}H resonance frequencies of Asn^{119}−Lys^{124}.

The HNCO spectrum allows identification of the sequential correlations between the CO($i - 1$) and the ^{15}N(i) and ^{1}H^N(i) resonances. The MQ-SE-(HACA)CO(CA)NH spectrum yields correlations between the ^{15}N(i) and ^{1}H^N(i) resonances and the CO(i) and CO($i - 1$) resonances. For the 2T delay value of 28.6 ms and as result of the generally smaller

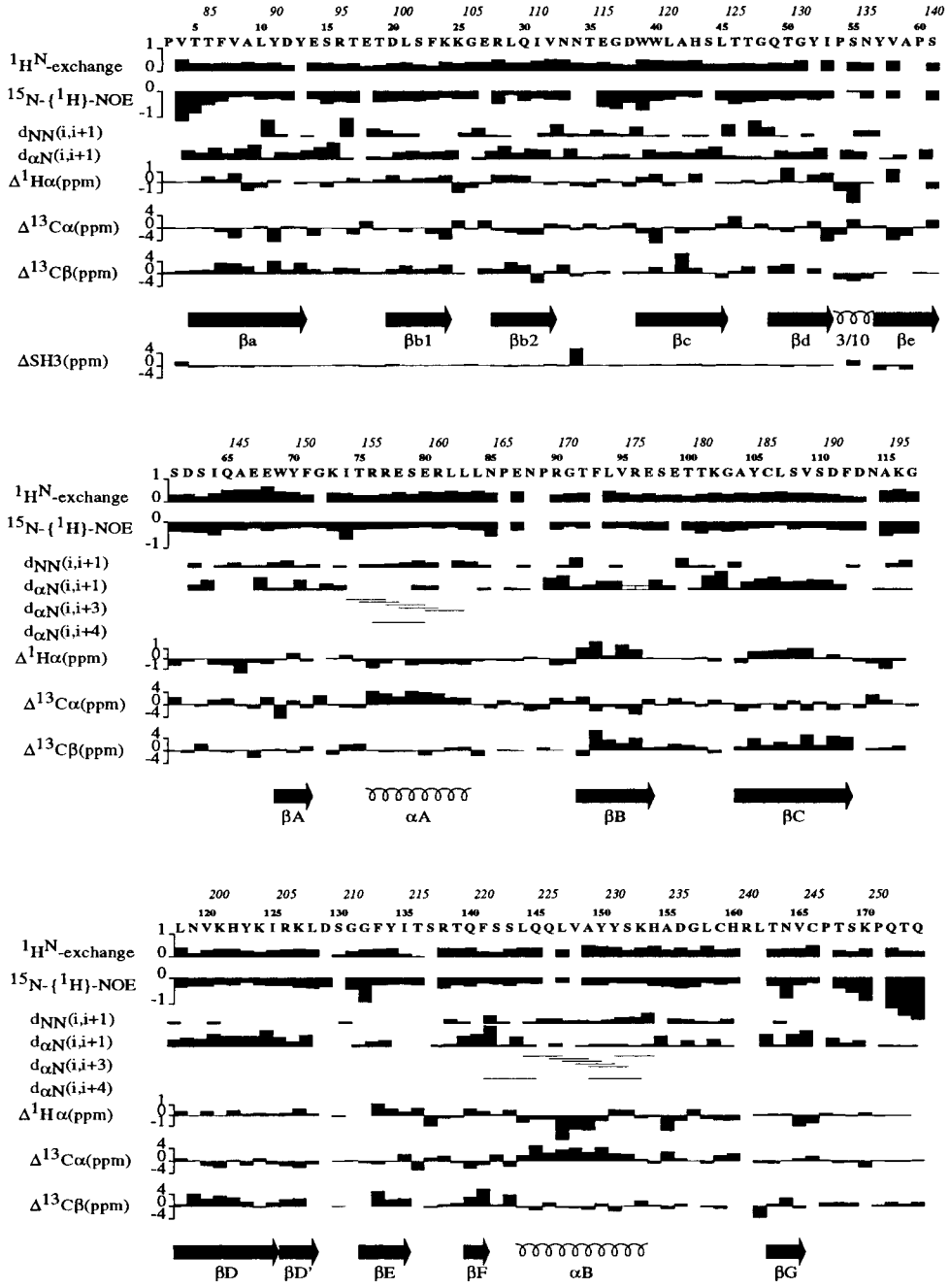

FIGURE 4: Summary of the saturation-transfer data, $^{15}N-\{^1H\}$ NOE data, sequential- and medium-range NOEs, and deviations from random-coil chemical shifts obtained for SH(32) as a function of residue number. Italic numbering refers to c-Src. Saturation-transfer data are plotted as I^{sat}/I, whereas heteronuclear NOE data are plotted as $(I^{sat} - I)/I$. Open bars denoting NOEs indicate experimental uncertainty due to partial overlap. Random coil values are listed relative to the values given by Wüthrich (1986) for H^α and by Spera and Bax (1991) for C^α and C^β. ΔSH3 denotes the differences in ^{15}N chemical shift relative to the values reported for the free SH3 domain by Yu et al. (1993).

$^2J(C^\alpha N)$ couplings with respect to the $^1J(C^\alpha N)$ couplings, the transfer to the CO(i) spin is favored and hence yields more intense cross peaks in the MQ-SE-(HACA)CO(CA)-NH spectrum. Note that this is the desirable situation since the correlations to the CO($i - 1$) are redundant as they are preferentially obtained from the HNCO spectrum. The combined use of the HNCO and MQ-SE-(HACA)CO(CA)-NH spectra yields an independent sequential link.

The data from the triple-resonance experiments listed in Table 1 in the supporting information were supplemented with the NOE data of the ^{15}N- and ^{13}C-separated NOE experiments to complete the sequential assignment procedure. The chemical shifts of H^N, ^{15}N, $^{13}C^\alpha$, H^α, $^{13}C^\beta$, and ^{13}CO are listed in Table 1 in the supporting information.

Analysis of Secondary Structure. The analysis of short- and medium-range NOEs together with the NMR parameters indicative for secondary structure, such as deviations from random coil chemical shifts $\Delta^{13}C^\alpha$, $\Delta^{13}C^\beta$, and Δ^1H^α, allow for identification of secondary structural elements. Figure 4 shows a summary of the saturation transfer data, $^{15}N-\{^1H\}$ NOE values, sequential- and medium-range $^1H-^1H$ NOEs, deviations from random coil chemical shifts, as well as ^1H and ^{15}N chemical shift changes upon phosphopeptide binding for residues Pro^3-Gln^{175} of our SH(32) polypeptide. Also shown in Figure 4 are the resulting secondary structural elements for this protein. Residues 4−170 of SH(32), corresponding to residues 83−249 in chicken pp60 c-Src, are ordered in solution as judged from the magnitude of the

saturation transfer with water, deviations from random coil chemical shifts, and $^{15}N-\{^1H\}$ NOE values. This region encompasses the residues corresponding to the SH3 domain (residues Val[4]−Ser[61]), the SH2 domain (residues Trp[69]−Val[165]), and also the seven-residue linker (residues Asp[62]−Glu[68]).

In all respects the data for the SH3 portion of our dual-domain protein indicate a structure very similar to that of the isolated c-Src SH3 domain in solution (Yu et al., 1992, 1993). The strong sequential $d_{\alpha N}$ NOEs together with the values for $\Delta^{13}C^{\alpha}$, $\Delta^{13}C^{\beta}$, and $\Delta^{1}H^{\alpha}$ are consistent with the formation of six β-strands in the SH3 domain**.** With the exception of βb_1, the six β-strands sequentially align with those observed in the isolated SH3 domain. Lys[24] at the end of βb_1 shows $d_{\alpha N}$, $\Delta^{13}C^{\alpha}$, $\Delta^{13}C^{\beta}$, and $\Delta^{1}H^{\alpha}$ values consistent with β-sheet formation and cross-strand NOEs to Asp[12] and Tyr[13] in the βa strand. In all but two cases an identical pattern of cross-strand NOEs is observed for the SH3 domain of SH(32), indicating a fold identical to that found in the isolated SH3 domain. This finding is further supported by a comparison of the ^{15}N chemical shifts reported for the isolated SH3 domain (Yu et al., 1993) and our data (Figure 4). Significant differences are found only for the C-terminal residues that are in close proximity to the SH2 domain of SH(32) and for Asn[34].

The structure of the linker region connecting the SH3 and SH2 domains is of great interest, since it will define the relative orientation of the two binding modules. Thus far, all dual-domain structures have been determined by X-ray crystallography and display different relative orientations of these domains. Our linker residues (Asp[62]−Glu[68]) are structured, as judged from the variation in intensity of sequential NOEs across this region, as well as the level of protection from saturation transfer with water, deviations of $^{13}C^{\alpha}$, $^{13}C^{\beta}$, and H^{α} chemical shifts from random-coil values, and the magnitude of $^{15}N-\{^1H\}$ NOE values. In addition, weak $d_{\alpha N}(i, i+2)$ NOEs are observed between residues Ser[61] and Ser[63] and between Ala[65] and Glu[67], indicating possible turnlike structure for residues in this region. This result is in contrast to the linker between the SH3 and SH2 domains in the Abl structural model, which consists of eight residues described as flexible (Gosser et al., 1995).

The NMR data of the residues corresponding to the SH2 domain of SH(32) are in accordance with the $\beta\alpha\beta\beta\beta\beta\beta\beta\alpha\beta$ topology also found for the X-ray and NMR structures of the human c-Src SH2 domain (Waksman et al., 1993; Xu et al., 1995). The data suggest some small differences between the SH(32) secondary structural elements and those defined by solution NMR for the isolated human c-Src SH2 (Xu et al., 1995). Our data indicate that helices αA and αB encompass residues Arg[76]−Leu[83] and Leu[144]−Lys[153], respectively, which would make them one residue shorter at both N- and C-termini when compared to the corresponding helices defined by Xu et al. (1995) for the isolated SH2. However, analysis of the refined average NMR structure of the isolated human c-Src SH2 domain (PDB code 1HCS) by the DSSP program (Kabsch & Sander, 1983) in fact indicates that helices αA and αB comprise residues Arg[76]−Leu[83] and residues Leu[144]−Lys[153], respectively, which is identical with our current NMR analysis as well as with the crystal structure of human c-Src SH2 (Waksman et al., 1993).

The large central β-sheet of the SH2 domain is formed by strands βB, βC, and βD. The NMR data are consistent with the presence of these β-stands, albeit that strand βC seems to extend through Phe[112]. The H^{α} of Phe[112] shows cross-strand NOEs to H^{α}(Leu[118]) and H^{N}(Asn[119]), consistent with antiparallel β-sheet formation. Also, the DSSP analysis of the refined average structure of the human c-Src SH2 indicates that Phe[112] is in a β-sheet conformation. Sequential $d_{\alpha N}$ NOEs, $\Delta^{1}H^{\alpha}$, $\Delta^{13}C^{\beta}$, and $\Delta^{13}C^{\alpha}$ data, and cross-strand NOEs indicate that β-strand DD′ runs from Leu[118] until Leu[128], which would extend this strand by one residue at both the N- and C-terminus compared with the analysis given by Xu et al. (1995) for the isolated SH2 domain. Again, our data are in accordance with the DSSP analysis of the refined average structure of SH2, whereas in the crystal structure of isolated SH2 the strand was defined from Asn[119] to Leu[128] (Waksman et al., 1993). The data further indicate formation of β-strands βA, βE, βF, and βG in accordance with the earlier results obtained for the isolated SH2 domain.

The NMR data of the human c-Src SH2 domain complexed to a phosphorylated pentapeptide (Xu et al., 1995) were recorded at different pH and salt concentration compared to the data used in the current study. Moreover, human c-Src SH2 has three amino acid substitutions relative to chicken c-Src SH2. Together, these differences make it less straightforward to assess structural differences from chemical shift arguments. Nevertheless, a comparison shows for most residues differences of less than 0.1 ppm and 0.3 ppm for H^{α} and C^{α} chemical shifts, respectively (data not shown). Regions with larger differences are found at the N- and C-termini of the SH2 domain, for the three nonconserved residues, and for residues preceding or following these three nonconserved residues. Smaller, but bigger than average, changes are found for the residues involved in peptide binding, such as those in the BC loop and in the βDD′ sheet.

The residues C-terminal of the βG strand show decreasing values of the $^{15}N-\{^1H\}$ NOE values, indicative of increasing mobility toward the C-terminus. However, the NOE and chemical shift data suggest that Cys[166]−Lys[170] still could possess some (transient) structure. In contrast, residues Pro[171]−Gln[173] show all characteristics of a highly mobile, flexible polypeptide. Therefore, in this soluble dual-domain system the SH2−kinase linker region [c-Src residues 246−254, which corresponds to residues 167−175 in the SH(32) construct] does not form a stable polyproline-II helical structure and does not bind in a stable manner to the SH3 domain, as was seen in the X-ray crystal structure of nearly intact Src (Xu et al., 1997).

Peptide Binding. In order to assess potential structural changes upon peptide binding to the SH2 domain of the SH(32) polypeptide we successively added one, two, and four molar equivalents of the high-affinity phosphopeptide EPQpYEEIPIYL[3] to a sample containing a 1 mM solution of uniformly ^{15}N-labeled SH(32) and monitored the changes in ^{15}N and ^{1}H chemical shifts by means of ^{15}N HSQC and three-dimensional ^{15}N NOESY-HSQC experiments. These chemical shifts provide a convenient parameter for assessing potential structural changes**,** in particular the loss, formation, or change in geometry of hydrogen bonds (de Dios et al., 1993; Le & Oldfield, 1994).

The changes in ^{1}H and ^{15}N chemical shifts upon complex formation are shown as a function of residue number in

[3] Peptide numbering is relative to the pY residue.

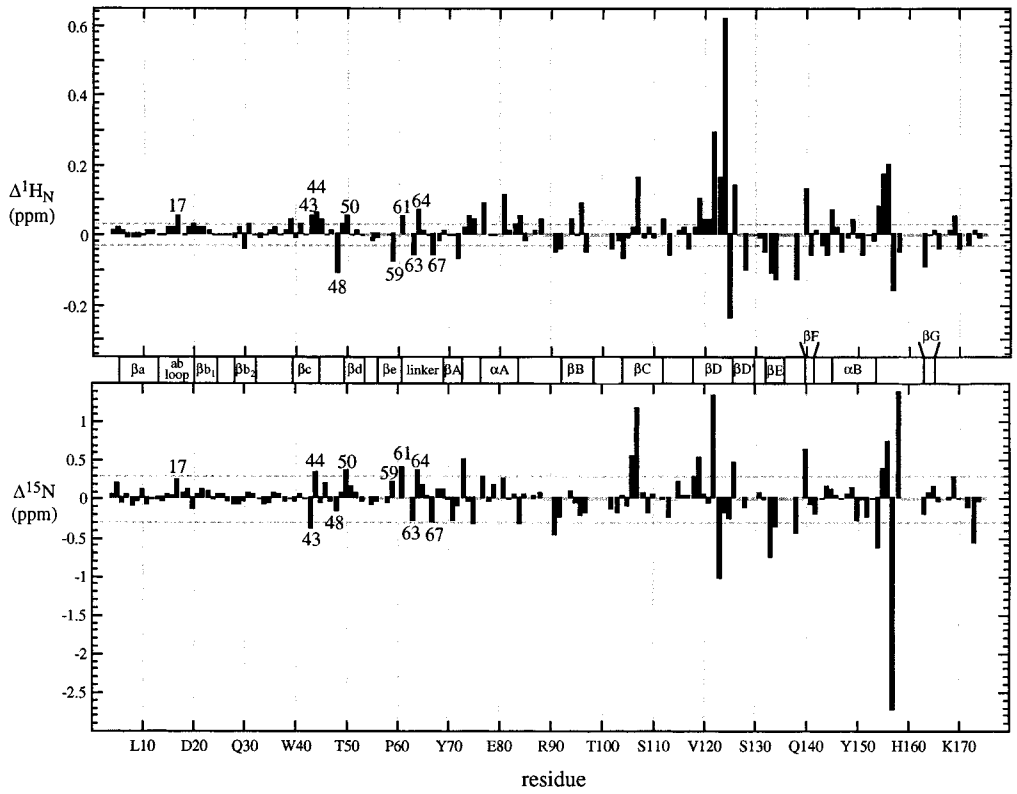

FIGURE 5: Changes in ^1H_N and ^{15}N chemical shift upon binding the phosphopeptide ligand NH_2-EPQpYEEIPIYL, plotted as a function of residue number. Elements of secondary structure are mapped between the two plots. Solid gray bars at 0 ppm in each plot indicate residues displaying either large changes in chemical shift or overlap that impaired unambiguous assignment or residues displaying a loss of the $^{15}N-^1H$ correlation due to chemical exchange broadening. Dashed gray horizontal lines at ± 0.03 ppm (Δ^1H_N plot) and ± 0.3 ppm ($\Delta^{15}N$ plot) illustrate cutoff values used to define significant changes in chemical shift. Residues not within the SH2 domain for which $\Delta^1H_N \geq \pm 0.05$ ppm are identified by residue number.

Figure 5. As expected, peptide binding strongly affects the chemical shifts of residues in the SH2 domain, in particular those in the βC, βDD′, and βE, and the BG loop regions. The c-Src SH2 binding pockets are formed by regions scattered throughout the domain and include residues in αA, βB, βC, βD, and βE and the BC, EF, and BG loops as illustrated in Figure 6. In all SH2/ligand structures determined thus far, the phosphotyrosine (pTyr) inserts into a large pocket and is stabilized by a network of hydrogen bonds and charge−charge interactions involving the aromatic pTyr ring and the phosphate oxygens. Src-SH2 structural determinants for pTyr peptide binding have been identified and include a bidentate interaction with the one Arg residue invariant across the SH2 kingdom (Arg^{96} in our construct) and amino−aromatic contacts with Arg^{76} and Lys^{124}, as well as polar interactions involving Ser^{108}, His^{122}, Ser^{98}, Thr^{100}, and Thr^{101}. Residues showing the largest changes are all known to interact with the peptide. As a specific example, the carbonyl oxygen of His^{122} makes a hydrogen bond to the backbone amide of Glu^{+1} of the peptide.

The second binding pocket presents a hydrophobic surface that interacts with a hydrophobic residue at the +3 position relative to the pTyr. The large change in chemical shift observed for Gly^{157} is also readily explained by the van der Waals interaction of the C^α of this residue with the methyl group of the Ile^{+3} residue of the peptide (Waksman et al., 1993). Large changes in chemical shift resulting in overlap and/or chemical exchange broadening were found in the BC and EF loops impairing unambiguous assignment of residues in this region. These two loops are known to exhibit the largest conformational changes upon complex formation (Waksman et al., 1993). The BC loop moves away from the protein core and thus opens the pY binding site, whereas the Ile binding site becomes more closed by changes in the EF loop.

In comparison, the chemical shift changes for most of the residues in the SH3 portion of SH(32) are relatively small (cf. Figure 5). However, small but significant changes (greater than 0.03 ppm and 0.3 ppm for ^1H and ^{15}N, respectively) are observed for certain residues. Specifically, Thr^{17}, His^{43}, Ser^{44}, Gly^{48}, Thr^{50}, Ala^{59}, Ser^{61}, Ser^{63}, Ile^{64}, and Glu^{67} show ^1H shifts of ± 0.05 or more upon ligand binding, and these same residues generally show the largest concomitant changes in ^{15}N chemical shift (all but four display shifts greater than $\pm$ 0.3 ppm). Empirical correlations and theoretical treatments have shown that ^1H_N chemical shifts are significantly affected by hydrogen-bond geometry, and ^{15}N chemical shifts are sensitive to local backbone and side-chain torsion angles as well as to direct (N−H) and indirect (C═O) hydrogen-bond geometry (de Dios et al., 1993; Le & Oldfield, 1994). SH3 residues that display the largest chemical shift changes are located in the ab loop (Thr^{17}), βc (His^{43} and Ser^{44}), the cd loop (Gly^{48}), βd (Thr^{50}), βe (Ala^{59} and Ser^{61}), and the linker region (Ser^{63}, Ile^{64}, and Glu^{67}), as illustrated in Figure 6. The relative location of these regions indicates a perturbation of chemical environment in the linker region that extends from one side of the SH3 domain to the other, possibly facilitated through side-chain interactions within the SH3 hydrophobic core.

We also probed the effects of peptide binding by comparing the saturation-transfer rates for the free and complexed forms of the SH(32) polypeptide. With the exception of

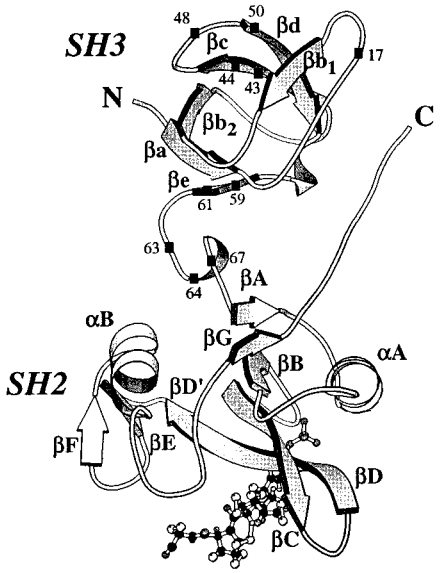

FIGURE 6: Ribbon diagram of SH(32) illustrating the backbone fold, the phosphopeptide binding region, and the location of residues not within the SH2 domain that exhibit significant amide proton chemical shift changes. The figure was generated using coordinates for the nearly intact Src X-ray crystal structure (Xu et al., 1997). Rasmol was used to generate the desired view, and the ribbon diagram was generated using Molscript (Kraulis, 1991). The approximate location of the phosphopeptide ligand is illustrated by inclusion of the ball-and-stick representation of the wild-type phosphotyrosine C-terminal tail. Residues in the SH3 domain or in the linker region for which $|\Delta^1H_N| \geq 0.05$ ppm are marked by black squares and are labeled with residue numbers.

Asp^{20} and Arg^{81}, the two forms of the SH(32) polypeptide had similar saturation transfer rates. This indicates a similar overall solvent accessibility for almost all residues.

In spite of the recent crystal structures of SH3-SH2 dual domain proteins (Nam et al., 1996; Maignan et al., 1995; Eck et al., 1994) and the crystal structures of the nearly intact Src and Hck proteins (Xu et al., 1997; Sicheri et al., 1997), the nature and extent of interdomain interactions in solution and their role in regulation in multidomain SH3-SH2 proteins is still not fully understood. Whereas the Lck SH(32) crystal structure suggests that head-to-tail dimerization plays an important role in modulation of SH2 ligand binding by the SH3 domain (Eck et al., 1994), the Abl crystal structure suggests that direct interactions between surface-exposed loops in each domain achieve this regulation (Nam et al., 1996), and the Grb2 crystal structure suggests independent functions of its SH2 and SH3 domains (Maignan et al., 1995). In contrast, in the crystal structures of nearly intact Src and Hck, interdomain communication is facilitated by the linker residues between the SH2 and kinase domains.

In the Lck SH(32) crystal structure, contacts of the pY^{+4} Pro and carboxyl-terminal end of the peptide with the ab loop of SH3 were postulated to be important for stabilization of the SH3−SH2 dimer and could explain the transforming potential of mutations in the c-Src ab loop (Eck et al., 1994). If these interactions were present in solution, large changes in chemical environment would be expected for residues in the ab loop, which would translate into large chemical shift changes. The chemical shift changes observed for these residues are not of the magnitude that would result from the above mode of dimer-mediated peptide binding (cf. Figure 4), in particular when compared with the significant effects observed for residues in the SH2 domain.

CONCLUSIONS

The results of heteronuclear NMR studies on the SH(32) polypeptide of chicken pp60 c-Src have been presented. Assignment of the backbone resonances was performed using heteronuclear triple-resonance experiments, in conjunction with the analysis of NOE data. The MQ-SE-(HACA)CO-(CA)NH experiment was presented, which improves the sensitivity of the original experiment by a factor 1.6−2.0. The correlations between intraresidual and sequential CO nuclei, the amide proton, and backbone nitrogen provided an additional independent sequential connectivity that greatly facilitated the assignment process.

Analysis of the NOE data in conjunction with other NMR parameters indicative of secondary structure indicates a very similar fold for both the SH3 and SH2 domains of SH(32) when compared to the solution and X-ray structures of the individual domains. This finding is corroborated by the small differences in chemical shift between the SH3 domain in SH(32) and the individual SH3 domain. For the SH2 domain of SH(32), differences in chemical shift with the individual human c-Src SH2 are readily explained in terms of amino acid substitutions between chicken and human c-Src and by the effects of peptide binding.

The linker region connecting the SH3 and SH2 domains is structured. NOEs indicative of a possible turnlike structure are observed that suggest a fixed relative orientation of the SH3 and SH2 domains. In contrast, the residues C-terminal to the SH2 domain, corresponding to the linker connecting the SH2 and kinase domains, are unstructured in the SH(32) polypeptide.

The binding of a high-affinity phosphorylated peptide to SH(32) predominantly perturbs the chemical shifts in the SH2 domain. The changes are readily explained in terms of the known mode of binding of a pY peptide with a SH2 domain. Small chemical shift changes are observed for residues in the SH3 domain that map onto a region including and spatially close to the linker between domains. These changes could correspond to minor conformational changes transmitted through the linker upon ligand binding and offer an intriguing possibility for a mechanism of cross-domain communication that could facilitate allosteric regulation between domains.

ACKNOWLEDGMENT

We thank Dr. Rolf Boelens and Professor Rob Kaptein for their stimulating interest and expert advice. We thank Chris Henkels for initial expression and purification studies, Ross Resnick for expert protein chemistry assistance, Professor Lewis Kay for use of his Varian pulse-sequence library, Michael Eck for providing the coordinates for the nearly intact c-Src crystal structure, Roger Sayle (Glaxo Wellcome) for use of the Rasmol program, Frank Delaglio (NIH/NIDDK) for use of nmrPipe and nmrDraw programs, Dan Garrett (NIH/NIDDK) for use of PIPP, Brian Whitehead for proofreading the manuscript, and the Cornell Biotechnology Protein/DNA Synthesis and Analysis Facility for mass spectrometry, N-terminal sequencing, analytical HPLC, and peptide synthesis services.

SUPPORTING INFORMATION AVAILABLE

Two tables listing ^{1}H, ^{13}C, and ^{15}N backbone and $^{13}C^{\beta}$ chemical shifts of SH(32) and experiments used for the assignment of SH(32) (5 pages). Ordering information is given on any current masthead page.

REFERENCES

Bax, A., & Ikura, M. (1991) *J. Biomol. NMR 1*, 99−104.

Booker, G. W., Breeze, A. L., Downing, A. K., Panayotou, G., Gout, I., Waterfield, M. D., & Campbell, I. D. (1992) *Nature 358*, 684−687.

Booker, G. W., Gout, I., Downing, A. K., Driscoll, P. C., Boyd, J., Waterfield, M. D., & Campbell, I. D. (1993) *Cell 73*, 813−822.

Boyd, J., Soffe, N., John, B., Plant, D., & Hurd, R. (1992) *J. Magn. Reson. 98*, 207−216.

Clubb, R. T., & Wagner, V. (1992) *J. Biomol. NMR 2*, 389−394.

Clubb, R. T., Thanabal, V., & Wagner, G. (1992a) *J. Biomol. NMR 2*, 203−210.

Clubb, R. T., Thanabal, V., & Wagner, G. (1992b) *J. Magn. Reson. 97*, 213−217.

Cohen, G. B., Ren, R., & Baltimore, D. (1995) *Cell 80*, 237−248.

Davis, A. L., Keeler, J., Laue, E. D., & Moskau, D. (1992) *J. Magn. Reson. 98*, 207−216.

Delaglio, F., Grzesiek, S., Vuister, G. W., Zhu, G., Pfeifer, J., & Bax, A. (1995) *J. Biomol. NMR 6*, 277−293.

de Dios, A. C., Pearson, J. G., & Oldfield, E. (1993) *Science 260*, 1491−1496.

Eck, M. J., Shoelson, S. E., & Harrison, S. C. (1993) *Nature 362*, 87−91.

Eck, M. J., Atwell, S. K., Shoelson, S. E., & Harrison, S. C. (1994) *Nature 368*, 764−769.

Feng, S., Chen, J. K., Yu, H., Simon, J. A., & Schreiber, S. L. (1994) *Science 266*, 1241−1247.

Fumagalli, S., Totty, N. F., Hsuan, J. J., & Courtneidge, S. A. (1994) *Nature 368*, 871−874.

Garrett, D. S., Powers, R., Gronenborn, A. M., & Clore, G. M. (1991) *J. Magn. Reson. 95*, 214−220.

Gosser, Y. Q., Zheng, J., Overduin, M., Mayer, B. J., & Cowburn, D. (1995) *Structure 3*, 1075−1086.

Griffey, R. H., & Redfield, A. G. (1987) *Q. Rev. Biophys. 19*, 51−82.

Grzesiek, S., & Bax, A. (1992a) *J. Magn. Reson. 96*, 432−440.

Grzesiek, S., & Bax, A. (1992b) *J. Am. Chem. Soc. 114*, 6291−6293.

Grzesiek, S., & Bax, A. (1992c) *J. Magn. Reson. 99*, 201−207.

Grzesiek, S., & Bax, A. (1993) *J. Am. Chem. Soc. 115*, 12593−12594.

Grzesiek, S., & Bax, A. (1995) *J. Biomol. NMR 6*, 335−339.

Hirai, H., & Varmus, H. E. (1990) *Mol. Cell. Biol. 10*, 1307−1318.

Hiroaki, H., Klaus, W., & Senn, H. (1996) *J. Biomol. NMR 8*, 105−122.

Hunter, T. (1987) *Cell 49*, 1−4.

Hunter, T. (1995) *Cell 80*, 225−236.

Ikura, M., Kay, L. E., & Bax, A. (1990) *Biochemistry 29*, 4659−4667.

Kabsch, W., & Sander, C. (1983) *Biopolymers 22*, 2577−2637.

Kato, J., Takeya, T., Grandori, C. G., Iba, H., Levy, J. B., & Hanafusa, H. (1986) *Mol. Cell. Biol. 6*, 4155−4160.

Kay, L. E., Keifer, P., & Saarinen, T. (1992a) *J. Am. Chem. Soc. 114*, 10663−10665.

Kay, L. E., Wittekind, M., McCoy, M. A., Friedrichs, M. S., & Mueller, L. (1992b) *J. Magn. Reson. 98*, 443−450.

Kay, L. E., Xu, G. Y., & Yamazaki, T. (1994) *J. Magn. Reson. A 109*, 129−133.

Kleywegt, G. J., Vuister, G. W., Padilla, A., Knechtel, R. M., Boelens, R., & Kaptein, R. (1993) *J. Magn. Reson. 102*, 166−176.

Kohda, D., Hatanaka, H., Odaka, M., Mandiyan, V., Ullrich, A., Schlessinger, J., & Inagaki, F. (1993) *Cell 72*, 953−960.

Koyama, S., Yu, H., Dalgarno, D. C., Shin, T. B., Zydowsky, L. D., & Schreiber, S. L. (1993) *Cell 72*, 945−952.

Kraulis, P. J. (1991) *J. Appl. Crystallogr. 24*, 946−950.

Kuriyan, J., & Cowburn, D. (1993) *Curr. Opin. Struct. Biol. 3*, 828−837.

Le, H., & Oldfield, E. (1994) *J. Biomol. NMR 4*, 341−348.

Lee, C.-H., Kominos, D., Jacques, S., Margolis, B., Schlessinger, J., Shoelson, S. E., & Kuriyan, J. (1994) *Structure 2*, 423−238.

Lin, P.-H., Shenoy, S., Galitski, T., & Shalloway, D. (1995) *Oncogene 10*, 401−405.

Löhr, F., & Rüterjans, H. (1995) *J. Biomol. NMR 6*, 189−197.

Maignan, S., Guilloteau, J. P., Fromage, N., Arnoux, B., Becquart, J., & Ducruix, A. (1995) *Science 268*, 291−293.

Marengere, L. E. M., Songyang, Z., Gish, G. D., Schaller, M. D., Parsons, J. T., Stern, M. J., Cantley, L. C., & Pawson, T. (1994) *Nature 369*, 502−505.

Marion, D., Ikura, M., & Bax, A. (1989) *J. Magn. Reson. 84*, 425−430.

McCoy, M. A., & Mueller, L. (1992) *J. Am. Chem. Soc. 114*, 2108−2112.

Moarefi, I., LaFevre-Bernt, M., Sicheri, F., Huse, M., Lee, C.-H., Kuriyan, J., & Miller, W. T. (1997) *Nature 385*, 650−653.

Muhandiram, D. R., & Kay, L. E. (1994) *J. Magn. Reson. B 103*, 203−216.

Murphy, S. M., Bergman, M., & Morgan, D. O. (1993) *Mol. Cell Biol. 13*, 5290−5300.

Musacchio, A., Noble, M., Pauptit, R., Wieringa, R., & Saraste, M. (1992) *Nature 359*, 851−855.

Musacchio, A., Saraste, M., & Wilmanns, M. (1994) *Struct. Biol. 1*, 546−551.

Nam, H. J., Haser, W. G., Roberts, T. M., & Frederick, C. A. (1996) *Structure 4*, 1105−1114.

Noble, M. E., Musacchio, A., Saraste, M., Courtneidge, S. A., & Wierenga, R. K. (1993) *EMBO J. 12*, 2617−2624.

Okada, M., Howell, B. W., Broome, M. A., & Cooper, J. A. (1993) *J. Biol. Chem. 268*, 18070−18075.

Overduin, M., Rios, C. B., Mayer, B. J., Baltimore, D., & Cowburn, D. (1992) *Cell 70*, 697−704.

Panchamoorthy, G., Fukazawa, T., Stolz, L., Payne, G., Reesquist, K., Shoelson, S., Songyang, Z., Cantley, L., Walsh, C., & Band, H. (1994) *Mol. Cell. Biol. 14*, 6372−6385.

Pascal, S. M., Singer, A. U., Gish, G., Yamazaki, T., Shoelson, S. E., Pawson, T., Kay, L. E., & Forman-Kay, J. D. (1994) *Cell 77*, 461−472.

Pawson, T. (1992) *Curr. Opin. Struct. Biol. 2*, 432−437.

Schaffhausen, B. (1995) *Biochim. Biophys. Acta 1242*, 61−75.

Seidel-Dugan, C., Meyer, B. E., Thomas, S. M., & Brugge, J. S. (1992) *Mol. Cell. Biol. 12*, 1835−1845.

Shaka, A. J., Keeler, J., Frenkiel, T., & Freeman, R. (1983) *J. Magn. Reson. 52*, 334−338.

Sicheri, F., Moarefi, I., & Kuriyan, J. (1997) *Nature 385*, 602−609.

Songyang, Z., Shoelson, S. E., Chaudhuri, M., Gish, G., Pawson, T., Haser, W. G., King, F., Roberts, T., Ratnofsky, S., Lechleider, R. J., Nell, B. G., Birge, R. B., Fajardo, J. E., Chou, M. M., Hanafusa, H., Schaffhauser, B., & Cantley, L. C. (1993) *Cell 72*, 767−778.

Songyang, Z., Shoelson, S. E., McGalde, J., Olivier, P., Pawson, T., Bostelo, R. X., Barbacid, M., Sabe, H., Hanafusa, H., Yi, T., Reu, R., Baltimore, D., Ramofsky, S., Feldman, R. A., & Cantley, L. C. (1994) *Mol. Cell. Biol. 14*, 2777−2785.

Spera, S., & Bax, A. (1991) *J. Am. Chem. Soc. 113*, 5490−5492.

Stonehouse, J., Shaw, G. L., Keeler, J., & Laue, E. D. (1994) *J. Magn. Reson. A 107*, 178−184.

Stover, D. R., Liebetanz, J., & Lyndon, N. B. (1994) *J. Biol. Chem. 269*, 26885−26889.

Superti-Furga, G., & Courtneidge, S. A. (1995) *BioEssays 17*, 321−330.

Superti-Furga, G., Fumagalli, S., Koegl, M., Courtneidge, S. A., & Draetta, G. (1993) *EMBO J. 12*, 2625−2634.

Taylor, S. J., & Shalloway, D. (1994) *Nature 368*, 867−871.

Taylor, S. J., Anafi, M., Pawson, T., & Shalloway, D. (1995) *J. Biol. Chem. 270*, 10120−10124.

Vuister, G. W., Boelens, R., Kaptein, R., Hurd, R. E., John, B., & van Zijl, P. C. M. (1991) *J. Am. Chem. Soc. 113*, 9688−9690.

Waksman, G., Kominos, D., Robertson, S. C., Pant, N., Baltimore, D., Birge, R. B., Cowburn, D., Hanafusa, H., Mayer, B. J., Overduin, M., Resh, M. D., Rios, C. B., Silverman, L., & Kuriyan, J. (1992) *Nature 348*, 636−653.

Waksman, G., Shoelson, S. E., Pant, N., Cowburn, D., & Kuriyan, J. (1993) *Cell 72*, 779−790.

Wittekind, M., & Mueller, L. (1993) *J. Magn. Reson. B 101*, 201−205.

Wüthrich, K. (1986) *NMR of Proteins and Nucleic Acids*, Wiley & Sons, New York.

Xu, R. X., Word, N., Davis, D. G., Rink, M. J., Willard, D. H., Jr., & Gampe, R. T. Jr. (1995) *Biochemistry 34*, 2107−2121.

Xu, W., Harrison, S. C., & Eck, M. J. (1997) *Nature 385*, 595−602.

Yoakim, M., Hou, W., Songyang, Z., Lui, Y., Cantley, L., & Schaffhausen, B. (1994) *Mol. Cell. Biol. 14*, 5929−5938.

Yu, H., Rosen, M. K., Shin, T. B., Seidel-Dugan, C., Brugge, J. S., & Schreiber, S.L. (1992) *Science 258*, 1665−1668.

Yu, H., Rosen, M. K., & Schreiber, S. L. (1993) *FEBS Lett. 324*, 87−92.

Zhu, G., & Bax, A. (1990) *J. Magn. Reson. 90*, 405−410.

BI9712044